AMD - Vol. 42

Solid Earth Geophysics and Geotechnology

presented at

THE WINTER ANNUAL MEETING OF
THE AMERICAN SOCIETY OF MECHANICAL ENGINEERS
CHICAGO, ILLINOIS
NOVEMBER 16-21, 1980

sponsored by

APPLIED MECHANICS DIVISION
THE AMERICAN SOCIETY OF MECHANICAL ENGINEERS

edited by

S. NEMAT-NASSER
NORTHWESTERN UNIVERSITY

THE AMERICAN SOCIETY OF MECHANICAL ENGINEERS
United Engineering Center 345 East 47th Street New York, N.Y. 10017

AN INCLUSION MODEL FOR PROCESSES PREPARATORY TO EARTHQUAKE FAULTING

J. W. Rudnicki
Department of Theoretical and Applied Mechanics
University of Illinois at Urbana-Champaign
Urbana-Champaign, Illinois

ABSTRACT

Predictions for processes preparatory to earthquakes based on an inclusion model of faulting are reviewed. The inclusion material is assumed to have properties representative of the response of brittle rock in compression; specifically, the inelastic response is strain softening, inhibited by hydrostatic compression and exhibits volume increase (dilation) due to shear. Strain softening of the inclusion material leads to a dynamic runaway of inclusion shear strain which is interpreted as the occurrence of an earthquake. For both dry and fluid-saturated rock masses, the model predicts that runaway instability is preceded by a period during which the rate of inclusion strain accelerates relative to the far-field strain rate. However, in a fluid-infiltrated rock mass, the coupling of the deformation with pore fluid diffusion causes a much more pronounced period of accelerating inclusion strain and delays the onset of instability beyond its occurrence in a dry rock mass. This transient stabilization arises from two mechanisms: the time dependent elastic response of the fluid-infiltrated material surrounding the inclusion and the dilatant hardening of the inelastic response of the inclusion material. The results for stabilization by dilatant hardening are shown to be consistent with recent laboratory experiments. The analysis is based on generalizations of Eshelby's results for inclusions to nonlinearly deforming inclusions and to a spherical inclusion embedded in a linear fluid-infiltrated elastic solid.

NOMENCLATURE

a	major semiaxis of ellipsoidal cavity or inclusion
b	minor semiaxis of ellipsoidal cavity or inclusion
c	diffusivity
$d^P\gamma$, $d^P\epsilon$	inelastic increments of shear and volume strain, respectively
e_{ij}	deviatoric strain
f	function giving time-dependence of shear strain of spherical cavity wall (see Figure 5)
g	acceleration of gravity
G	shear modulus
h	hardening modulus
K	drained value of bulk modulus
K_f, K_s	bulk modulus of pore fluid and solid constituents, respectively
K_s'	an additional modulus of a porous elastic solid
K', K_f'	effective values of bulk moduli due to dilatant hardening
κ, k, k	permeabilities
L	effective fault length in dislocation model of (7)
$L_{ijk\ell}$	tensor of elastic moduli
M	elastic modulus, $K/(1 + 3K/4G)$
m	fluid mass content per unit volume of porous solid
$\underline{n}$	inward unit normal to cavity boundary
p	pore pressure
q_i	mass flow rate in x_i direction per unit area
$Q_{ijk\ell}$	factors relating applied traction to strain at cavity wall (1)
Q, R	nondimensional driving forces proportional to $\dot{\tau}_\infty$
$S_{ijk\ell}$	array of shape factors used in Eshelby's inclusion solution
S_{ij}	deviatoric tensor ($S_{kk} = 0$)
t	time
t_D	diffusion time a^2/c for spherical inclusion
v	apparent volume fraction of pore fluid
x_i	coordinate
α	relaxation constant
β	dilatancy factor
γ	engineering shear strain
γ_p, γ_o	strain at peak stress and elastic limit, see Figure 2
$\gamma_{B'}$, $\gamma_{D'}$	values of inclusion shear strain at runaway under drained and undrained conditions, respectively
Γ	measure of far-field strain rate
δ	relative slip on frictional fault surface
δ^*	relative slip necessary to reduce shear stress from τ_p to τ_r
δ_{ij}	Kronecker delta, $\delta_{ij} = 1$ if $i = j$, $\delta_{ij} = 0$ if $i \neq j$
ε_{ij}	strain
ϵ	volume strain, ε_{kk}
μ	friction coefficient
ν_e, ν, ν_u	effective, drained and undrained values of Poisson's ratios, respectively
λ	$\gamma_p - \gamma_o$, half width of peak in inclusion stress strain curve
τ	shear stress
τ_p	peak values of shear stress

$\Delta\tau$	difference between peak and residual values of friction stress
ρ	mass density of pore fluid
σ_{ij}	stress
σ	mean normal stress (positive in compression), $\sigma = -\sigma_{kk}/3$
σ_c	confining stress in axisymmetric compression test
$\bar{\sigma}_c$	confining stress minus pore fluid pressure
θ	time non-dimensionalized by diffusion time
ξ, ξ_u	shape factors for drained and undrained response
ζ	$1 - K/K_s'$

Subscripts and superscripts

∞	denotes value in far field
inc	denotes value in inclusion
prec	denotes percursor time
rev	denotes value in reservoir

INTRODUCTION

In recent years there has been much attention given to the possibility that earthquakes can be predicted. To determine whether prediction is possible and, if possible, to make predictions on a rational basis, an improved understanding of processes preceding earthquakes is needed. This paper reviews recent results based on an inclusion model of earth faulting which is mechanically consistent and incorporates material behavior representative of fissured rock. This model predicts that dynamic instability, which is interpreted as the occurrence of an earthquake, is preceded by a period of accelerating strain. Moreover, the coupling of deformation with the diffusion of an infiltrating pore fluid can delay the onset of dynamic instability, set the time scale of the failure process, and cause a more pronounced precursory period of accelerating strain. The time scale and character of this accelerating deformation are such that observable precursors, for example, accelerated strain or tilt of the ground surface, changes in local pore fluid pressure, and in physical properties such as electrical resistivity, radon content of wells, or seismic wave speed ratios, are possible. Some discussion of these results has also been included in recent reviews of the theory of precursory processes in earthquake rupture (1) and the mechanics of earthquake rupture (2).

The inclusion model of earth faulting (3) considers a zone (the inclusion) having mechanical properties which are uniform but different from those of the surrounding material. Specifically, the inclusion is assumed to undergo inelastic deformation representative of brittle rock in compression whereas the surrounding material is regarded as nominally linear elastic. In compression, the stress-strain curve of brittle rock typically exhibits a peak, i.e., brittle rock is strain softening, and inelastic shearing is inhibited by hydrostatic compression and accompanied by inelastic volume increase (dilation). The inclusion may idealize either a weakened zone of material (3) which, because of past faulting, has a lower threshold to inelastic behavior or a "seismic gap" (1) which is driven into the regime of inelastic behavior because it lags behind the surrounding material in its adjustment to the imposed far field deformation. In either case, continued loading of the rock mass drives the inclusion material into the strain softening regime. If the slope of the descending stress strain curve becomes sufficiently negative, further quasistatic deformation is not possible and a dynamic runaway of inclusion shear strain occurs. This instability is analogous to that which occurs in a compliant testing machine if the load carrying capacity of the sample decreases more rapidly than the machine can unload.

Rice (1) has pointed out that a general feature of this class of models (and of frictional models based on sliding on a discrete surface in which the friction stress decreases with sliding distance; see, for example, (4, 5, 6, 7) and the article by Stuart in this volume.) is the increase, prior to instability, of the ratio of inclusion strain increment to far-field strain increment. Although this increase may give rise to observable precursors, Rice et al. (8) and Rice and Rudnicki (9) (hereafter, this reference will be abbreviated as RR) have shown that if the rock mass is fluid-infiltrated, the coupling of deformation to the diffusion of pore fluid can stabilize the rock mass and give rise to a more pronounced period of accelerated deformation. This stabilization is, however, transient and ultimately culminates in instability, although its onset is delayed beyond the occurrence in the absence of pore fluid.

The stabilization by pore fluid effects results from the fact that both the inelastic response of the inclusion and the elastic response of the surrounding material are stiffer for rapid load alterations. More precisely, "rapid" means too rapid to allow time for fluid mass diffusion from material elements and such conditions are said to be undrained. Alternatively, drained conditions occur when load alterations are slow enough that changes in pore fluid pressure are alleviated by fluid mass diffusion. It is well known from analyses of consolidation in soil mechanics (e.g., (10), (11)) that the stiffness of a fluid-infiltrated, but otherwise elastic, material is greater for undrained conditions than for drained conditions. The effects of this time-dependent elastic response on faulting have been discussed by Rice and Cleary (12), Booker (13), Rice and Simons (14), Rice et al. (8), and RR (9) (Also, see the article by Rice in this volume), and Ruina (15) has discussed the retardation of hydraulic fracture by this effect. The source of the increased stiffness of inelastic response is the tendency of brittle rock to dilate or increase its pore space when sheared inelastically. For undrained conditions, this dilation tends to cause a decrease in the local pore fluid pressure and, consequently, an increase in the effective compressive stress, that is, the total stress minus the pore fluid pressure. Because the inelasticity of brittle rock arises from microscale processes which are frictional in nature, this increase in effective compressive stress inhibits further inelastic deformation. This phenomenon is called dilatant hardening and was first discussed for granular media by Reynolds (16). Frank (17) was the first to discuss its relevance of this effect to faulting and Brace and Martin (18) and Martin (19) have observed dilatant hardening in laboratory deformation of rock. Further analyses of dilatant hardening have been given by Rice (20, 1), Rudnicki (21), and RR.

The analysis of the inclusion model of faulting is based on generalizations of Eshelby's (22, 23) results for ellipsoidal inclusions in linear elastic solids. In the absence of coupling of the deformation with pore fluid diffusion, the generalization is the modest one of recognizing that Eshelby's results can be used to relate the stress and strain in the inclusion to the stress and strain applied in the far-field regardless of whether the inclusion is elastic or inelastic so long as it is homogeneous. For the coupled deformation diffusion problem, the generalization is a more substantial one and to date has been accomplished only for

spherical inclusions by Rice, Rudnicki and Simons (8). Their derivation is based on the solution for a spherical cavity in a fluid infiltrated solid loaded by tractions at the cavity boundary.

Of course, the inclusion model of faulting will not be appropriate for all circumstances. Because of kinematic constraints or continued faulting in the same region, inelastic deformation associated with faulting may be confined to a narrow zone or fault surface. In this case, a model of faulting as a spreading crack-like zone of slip may be more appropriate (e.g., (14), (1), Rice, this volume). Nevertheless, even though faulting is often idealized as slip on a distinct surface or intense shear of a narrow zone, this may be the result of localization of inelastic deformation in a much larger volume. Indeed observations of changes of physical properties prior to earthquakes at relatively large distances from the fault suggest such an extent of inelastic deformation.

The review first considers the inclusion model and the application of Eshelby's results to the analysis of runaway instability. Then the effects of fluid-infiltration are reviewed and the recent experimental observations of Martin (19) are discussed in terms of the analysis of RR.

INCLUSION MODEL AND RUNAWAY INSTABILITY

First the case in which the rock mass is dry or deforms under drained conditions is considered. As already mentioned, under drained conditions the deformation occurs so slowly that alterations of pore fluid pressure are alleviated by diffusive mass flux. Of course, if the rock mass is fluid-infiltrated, such conditions will not apply near instability.

The analysis of runaway instability is based on recognizing that Eshelby's (22) results, although originally obtained for elastic inclusions, can be used to relate the stress and strain in an inelastic inclusion to the stress and strain applied in the far field. This result can be obtained by first considering a cavity in an infinite linear elastic solid having moduli $L_{ijk\ell}$. The solid is loaded at the cavity boundary by uniform tractions $n_i \sigma_{ij}$ where n_i are the components of the unit normal directed inward from the cavity boundary. Eshelby (22) demonstrated that if the cavity is ellipsoidal, the cavity boundary deforms as if the interior had undergone a uniform strain ϵ_{ij} which is given by

$$\epsilon_{ij} = Q_{ijk\ell}\, \sigma_{k\ell} \tag{1}$$

where the $Q_{ijk\ell}$ depend on the elastic constants and the geometry of the cavity.

Eshelby (22) actually obtained this result by a different route. He first considered an ellipsoidal region ("the inclusion") of a linear elastic solid to undergo a change of size and shape which, in the absence of constraint by the surrounding matrix, would be given by the homogeneous stress-free transformation strain ϵ^T_{ij}. He then showed that the strain which results in the inclusion due to the presence of the constraint by the matrix is also homogeneous and is related to ϵ^T_{ij} by

$$\epsilon_{ij} = S_{ijk\ell}\, \epsilon^T_{k\ell}$$

where the $S_{ijk\ell}$ are factors which depend on the shape of the ellipsoid and on ratios of the elastic constants of the matrix. Because the resulting strain of the inclusion is homogeneous, Eshelby (22) was also able to solve problems for inclusions having elastic constants different from those of the matrix and, hence, for cavities. The $Q_{ijk\ell}$ are related to the $S_{ijk\ell}$ by the following expression (21)

$$1 = L_{ijpq}\, [\delta_{pk}\, \delta_{q\ell} - S^{-1}_{pqk\ell}]\, Q_{k\ell mn}$$

where $S^{-1}_{pqk\ell}\, S_{k\ell ij} = \delta_{pj}\, \delta_{qj}$. General expressions for $S_{ijk\ell}$ have been given by Eshelby (22, 23) and these have been recorded by Rudnicki (3). Rudnicki (3) has also recorded the expressions for the $S_{ijk\ell}$ in the special case of axisymmetric ellipsoids and has tabulated their values for various aspect ratios.

The solution for an ellipsoidal inclusion of homogeneous material which is embedded in an infinite linear elastic body subjected to uniform stress or strain at infinity can be constructed by using (1) and superposition. In particular, the field outside the inclusion is identical to that which results from the sum of the following: (i) uniform stress σ^∞_{ij} and the strain associated with σ^∞_{ij} by

$$\sigma^\infty_{ij} = L_{ijk\ell}\, \epsilon^\infty_{k\ell} \tag{2}$$

and (ii) fields which result from loading the cavity boundary by the following tractions

$$n_j\, \sigma_{ji} = n_j\, (\sigma^\infty_{ji} - \sigma^{inc}_{ji}). \tag{3}$$

The displacements of the cavity boundary which result from (ii) must be consistent with uniform strain of the interior given by

$$\epsilon_{ij} = \epsilon^{inc}_{ij} - \epsilon^\infty_{ij} \tag{4}$$

Because these strains must be related to the loading (3) by (1), the result is the following "Eshelby relation"

$$\epsilon^{inc}_{ij} - \epsilon^\infty_{ij} = Q_{ijk\ell}\, (\sigma^\infty_{k\ell} - \sigma^{inc}_{k\ell}) \tag{5}$$

where ϵ^{inc}_{ij} and σ^{inc}_{ij} can now be identified as the strain and stress of the inclusion material. Note that (5) has been constructed without reference to the constitutive law of the inclusion material and requires only that the inclusion material be homogeneous, the inclusion shape be ellipsoidal, and the surrounding matrix be linearly elastic.

Runaway instability is best illustrated by considering the special case of pure shear and using a graphical construction due to Rice (1, 8). The component of (5) for pure shear is

$$\gamma_{inc} - \gamma_\infty = (\xi/G)\, [\tau_\infty - \tau_{inc}] \tag{6}$$

where γ is the engineering shear strain, G is the shear modulus of the surrounding material (assumed, for convenience, to be isotropic) and ξ is a shape factor which depends on Poisson's ratio and the geometry of the inclusion.

The value of ξ for a spherical inclusion is (22)

$$\xi = 2(4 - 5\nu)/(7 - 5\nu), \tag{7a}$$

where ν is Poisson's ratio for the matrix material. For flat axisymmetric and cylindrical inclusions of aspect ratio $a/b \gg 1$, the values of ξ are

$$\xi = (a/b)\, [4(1 - \nu)/\pi(2 - \nu)] \tag{7b}$$

and

$$\xi = (a/b)(1 - \nu)/\pi \qquad (7c)$$

respectively ((3) with correction noted in (1)). For $\nu = 0.2$, $\xi = 1.0$ for the spherical inclusion and $\xi = 10$ for the axisymmetric inclusion with $a/b \simeq 18$.

Equation (6) is plotted in Figure 1 as the Eshelby line of slope $-G/\xi$. Also shown is the (linear elastic) constitutive law for the surrounding material $\tau_\infty = G\gamma_\infty$ and a relation for the inclusion shear stress τ_{inc} as a function of the inclusion shear strain γ_{inc}. The latter is drawn to be representative of the behavior of brittle rock in compression. For a given value of τ_∞, corresponding to point A in Figure 1, the corresponding values of τ_{inc} and γ_{inc} are given by the intersection (A') of the Eshelby line through point A with the inclusion stress-strain curve. As τ_∞ is increased, the Eshelby line moves outward parallel to itself until it is tangent to the inclusion stress strain curve at B'. At this point, any further increase in τ_∞ cannot be accommodated by quasistatic deformation and a dynamic runaway of inclusion shear strain occurs. Hence, the condition for runaway instability is the following:

$$d\tau_{inc}/d\gamma_{inc} = -G/\xi \qquad (8)$$

Equation (6) can be expressed in differential form as

$$d\gamma_{inc}/d\gamma_\infty = (1 + \xi)\,[1 + (\xi/G)\,d\tau_{inc}/d\gamma_{inc}]^{-1} \qquad (8a)$$

and, in this form, it is clear that the condition (8) corresponds to the ratio $d\gamma_{inc}/d\gamma_\infty$ becoming unbounded. Furthermore, if $d\tau_{inc}/d\gamma_{inc}$ decreases continuously, the approach to instability will be marked by a continuous increase in the ratio on the left hand side of (8a).

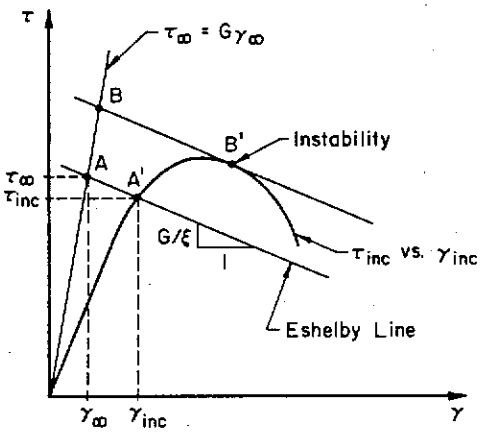

Figure 1. Graphical illustration of runaway instability. (After Rice (1)).

As a specific example, consider the following relation for τ_{inc} versus γ_{inc} which was used by RR in their numerical calculations:

$$\tau_{inc} = G\gamma_{inc}, \quad \gamma_{inc} \le \gamma_o$$
$$\tau_{inc} = \tau_p - G(\gamma_{inc} - \gamma_p)^2/2\lambda, \quad \gamma_{inc} \ge \gamma_o \qquad (9)$$

where γ_o is the strain at the elastic limit, and $\gamma_p = \gamma_o + \lambda$ is the strain at peak stress τ_p (Figure 2). Using (9) and $\tau_\infty = G\gamma_\infty$ in (6) yields an expression for γ_{inc} as a function of γ_∞. In Figure 2 the postpeak variation of γ_{inc} (divided by its value at instability, $\gamma_{inc} = \gamma_p + \lambda/\xi$) is plotted against the following measure of far field strain:

$$\Gamma = 2\xi[\gamma_\infty (1 + \xi) - \xi\tau_p/G - \gamma_p]/\lambda$$

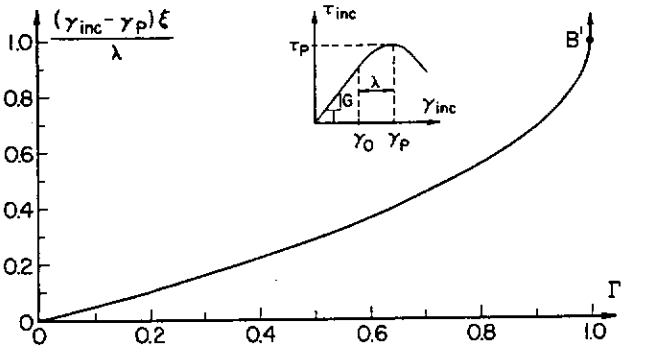

Figure 2. Postpeak variation of inclusion strain as a function of far field strain (as measured by Γ) for inclusion stress strain curve used by RR (see (9)) and shown as inset.

Clearly, the ratio $d\gamma_{inc}/d\gamma_\infty$ increases as instability is approached and as noted by Rice (1), this feature is a general precursory effect for strain softening models. Of course, in the earth's crust γ_∞ changes extremely slowly (In California, measured strain rates are typically less than 1 μ strain per year (24, 25)) and hence the acceleration of inclusion strain may not be detectable until very near instability.

In the model of (3) the inclusion was regarded as weaker than the surrounding material ($\tau_{inc} < \tau_\infty$) and Figure 1 has been drawn to be compatible with this interpretation. However, Rice (1) has shown that similar constructions can be applied to a seismic gap, that is, an inclusion zone which has lagged behind the surrounding material in adjusting to the far field deformation, and to sliding on frictional surfaces for which the friction stress is a function of the amount of relative sliding (also see (7)).

Because brittle rock tends to dilate when sheared inelastically, and because dilation of the inclusion material must occur against the constraint of the surrounding matrix, the response in shear is in general coupled to that for hydrostatic compression. Consequently, the τ_{inc} versus γ_{inc} curve which is illustrated schematically in Figure 1 should be regarded as that appropriate for in situ behavior. Rudnicki (3), in his treatment of runaway instability for arbitrary ellipsoidal inclusions and general loading conditions, has also given a full analysis of the effects of this coupling between shear and hydrostatic compression. Rudnicki (3) used a version of the constitutive law proposed by Rudnicki and Rice (26) to model the behavior of brittle rock and the next section reviews this law for the simple deformation state which is a combination of pure shear and hydrostatic compression. This constitutive law will then be used to illustrate the inhibiting effects of pressure sensitive and dilatant behavior on runaway instability for a spherical inclusion.

Constitutive Law for Inclusion Material

The constitutive relation discussed here is a variation of that developed by Rice (20) for an analysis of the stability of dilatant hardening and generalized by Rudnicki and Rice (26) to multiaxial loading and arbitrary deformation magnitudes. Consider a small element

of the inclusion material which is subjected to a combination of hydrostatic stress σ (in compression) and shear stress τ. If the next increment of deformation tends to cause elastic unloading, the strain increments which are work conjugate to σ and τ are given by

$$d\gamma = d\tau/G, \quad d\varepsilon = -d\sigma/K \tag{10}$$

where G and K are the elastic shear and bulk moduli, respectively. If instead the next increment of deformation tends to cause continued inelastic deformation, the inelastic increments of strain must be added to those of (10). For constant hydrostatic stress ($d\sigma = 0$), the inelastic increment of shear strain is

$$d^P\gamma = d\tau/h \tag{11}$$

where the modulus h may be positive (hardening) or negative (softening) and is related to the slope of the τ versus γ curve by

$$d\tau/d\gamma = h/(1 + h/G) \quad \text{for} \quad d\sigma = 0 \tag{12}$$

Because the inelasticity of brittle rock is primarily due to microscale processes which are frictional in nature (e.g., frictional sliding on fissure surfaces and microcracking from the tips of pre-existing fissures), inelasticity is inhibited by an increase in hydrostatic compression. Consequently, for increments in which $d\sigma \neq 0$, $d\tau$ is replaced in (11) by $d\tau - \mu d\sigma$ where μ is a coefficient of friction which expresses the elevation of the flow stress due to hydrostatic compression. Uplift in sliding over asperities and tensile cracking from the tips of existing fissures give rise to macroscopic inelastic volume increase (dilatancy) accompanying inelastic shear strain. Hence, the ratio between inelastic increments of volume strain and shear strain is presumed to be fixed by the current stress state:

$$d^P\varepsilon = \beta d^P\gamma \tag{13}$$

where β is the dilatancy factor. In terms of a "yield surface" in τ versus σ space, μ is the local slope of the yield surface and $\tan^{-1}(\beta - \mu)$ is the angle between the inelastic strain increment plotted as a vector $(-d^P\varepsilon, d^P\gamma)$ and the normal to the yield surface. Rice (20), Rudnicki and Rice (26), and Rudnicki (3) have estimated values of μ in the range 0.5 to 1.0 and β in the range 0.2 to 0.5 from experimental results. In general, all the parameters of the constitutive law may change with deformation but the variation in h is typically most rapid. Cleary and Rudnicki (27) have given an expression for the tangent modulus in axisymmetric compression in terms of h, μ, β and elastic moduli.

The constitutive law, now written in rate form, for continued inelastic deformation is

$$\dot\gamma_{inc} = \dot\tau_{inc}/G + (\dot\tau_{inc} - \mu\dot\sigma_{inc})/h \tag{14}$$

$$\dot\varepsilon_{inc} = -\dot\sigma_{inc}/K + \beta(\dot\tau_{inc} - \mu\dot\sigma_{inc})/h \tag{15}$$

where the designation "inc" has been included explicitly. Deformation which tends to make $\dot\tau_{inc} > \mu\dot\sigma_{inc}$ corresponds to continued inelastic deformation whereas that which tends to make $\dot\tau_{inc} < \mu\dot\sigma_{inc}$ corresponds to elastic unloading.

Runaway Instability for a Spherical Inclusion

For a spherical inclusion, the Eshelby relations (5) for deviatoric and hydrostatic components decouple. These equations reduce to the following simple expressions

$$\dot\varepsilon_{inc} - \dot\varepsilon_\infty = (3/4G)[\dot\sigma_{inc} - \dot\sigma_\infty] \tag{16}$$

$$\dot\gamma_{inc} - \dot\gamma_\infty = (\xi/G)[\dot\tau_\infty - \dot\tau_{inc}] \tag{17}$$

where $\xi = 2(4 - 5\nu)/(7 - 5\nu)$, $\sigma = -\sigma_{kk}/3$, $\varepsilon = \varepsilon_{kk}$ and it has been assumed following Rudnicki (3) that (5) can be used to relate rates of stress and strain. Using (15) and (16) to eliminate σ_{inc} from (17) yields

$$\dot\gamma_{inc} = \dot\tau_{inc}/G + \dot\tau_{inc}/(h + \mu\beta M) \tag{18}$$

where $M = K/(1 + 3K/4G)$ and, for convenience, it has been assumed that $\dot\varepsilon_\infty = 0$. This equation makes clear the inhibiting effect that the constraint of the surrounding material has on inelastic deformation of the inclusion: Comparison with (11) reveals that the hardening modulus is elevated from h to an effective value $h + \mu\beta M$. The condition for runaway instability is easily obtained from (8):

$$h = -G/(1 + \xi) - \mu\beta K/(1 + 3K/4G). \tag{19}$$

It is evident from (19) that for a spherical inclusion runaway instability is predicted to occur well after peak stress, that is, when the hardening modulus is less than zero and comparable in magnitude to the elastic shear modulus. Although, as mentioned earlier, runaway is predicted to occur closer to peak stress for narrow inclusions, this calculation and the more general analysis of (3) indicate the importance of strain-softening behavior in giving rise to instability. It has sometimes been suggested, primarily on the basis of a comparison by Walsh (28) of the effective stiffness of a loading apparatus with that of the material surrounding a fault, that such postpeak deformation would not be realized in situ. However, the calculation by Walsh (28) of the effective stiffness of a fault assumed slip on a crack-like surface and elastic properties of the fault zone. Although the analysis of (3) agrees with that of (28) in the limiting case of an infinitesimally thin inclusion of nondilatant properties, it is clear that more generally dilatancy, pressure-sensitivity of inelastic behavior, and a finite thickness of the inclusion contribute to the requirement that runaway instability occur after peak stress.

Equation (19) assumes that the elastic moduli of the inclusion are equal to those of the surrounding material. However, the microcracking which gives rise to inelastic deformation of brittle rock also causes a degradation of the elastic moduli to 50 to 90% of their initial values (3). If the elastic moduli of the inclusion are G^* and K^*, then Rudnicki (21) has shown that the value of h at runaway instability is

$$h = -G^*/(1 + \xi G^*/G) - \mu\beta K^*/(1 + 3K^*/4G). \tag{19a}$$

For $G^* \ll G$ and $K^* \ll K$, the expression in the denominator of each term reduces to unity. Rudnicki (21) also considered the limiting case of an extremely anisotropic spherical inclusion which could deform only by shear and compression or extension relative to a single direction. In this case runaway instability was predicted always to occur after that for the isotropic inclusion.

Rudnicki (3) also used the analysis of (26) to consider the possibility that deformation in the inclusion would cease to be homogeneous and further deformation would be concentrated in a narrow zone. Rudnicki (3) concluded that conditions for localization of

deformation would, in general, be met prior to those for runaway instability although for very narrow zones both conditions may be satisfied nearly simultaneously. This conclusion was based primarily on the observation that for nearly spherical inclusions the mode of deformation in the inclusion, for example, plane strain versus axisymmetric compression, would be nearly the same as that imposed in the far field whereas for very narrow inclusions the mode of deformation is constrained to be essentially a combination of pure shear and uniaxial compression. A more detailed analysis of conditions for localization of deformation in general ellipsoidal inclusions would be useful. Because conditions for localization of deformation are typically met prior to runaway instability, the constitutive law of the inclusion material should be regarded as reflecting the overall response of the inclusion rather than that of any specific homogeneous material.

EFFECTS OF COUPLED DEFORMATION AND DIFFUSION

If near surface crustal rock is infiltrated with ground water, predictions of runaway instability based on drained conditions will be altered by coupling between deformation and pore fluid diffusion. More specifically runaway instability may be stabilized by the two mechanisms which were mentioned earlier: time dependent stiffness of the material surrounding the inclusion and dilatant hardening. The stabilizing effects of these mechanisms can be illustrated in terms of the graphical construction in Figure 1 (1).

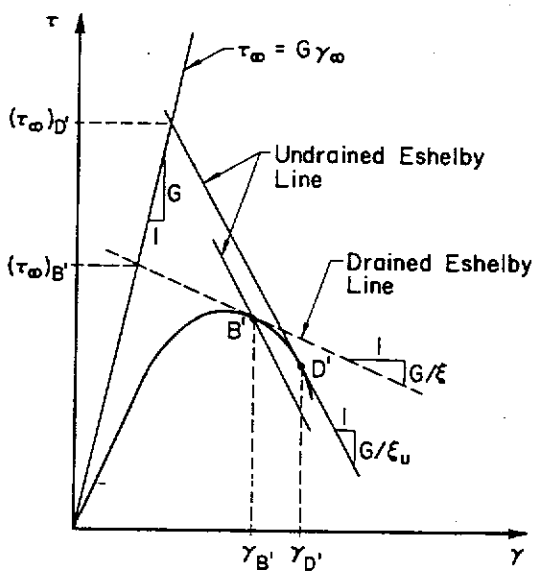

Figure 3. Graphical illustration of stabilization by time dependent stiffness of material surrounding the inclusion. Instability is delayed from B' to D'. Stiffness changes are greatly exaggerated for illustration.

Figure 3 illustrates stabilization by the time dependent stiffness effect. The Eshelby line for drained response is shown as the dashed line of slope $-G/\xi$ which is tangent to the inclusion stress strain curve at B'. However, the rapid acceleration of inclusion strain which occurs as B' is approached (as illustrated in Figure 2) will elicit undrained response. Because the surrounding material is elastically stiffer for undrained response, the corresponding Eshelby line is steeper and is not tangent to the inclusion stress strain curve at B'. Consequently, instability will not occur at B'. but instead, is delayed to D' where continued softening of the inclusion material has caused the stress strain curve to become tangent to the Eshelby line for undrained response. During this period the inclusion strain increases from $\gamma_{B'}$ to $\gamma_{D'}$.

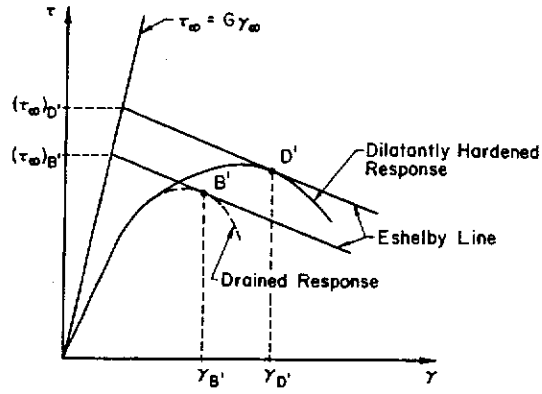

Figure 4. Graphical illustration of stabilization by dilatant hardening of inclusion material. Instability is delayed from B' to D'. Magnitude of the dilatant hardening effect is greatly exaggerated for illustration.

Figure 4 illustrates stabilization by dilatant hardening. Here the slope of the Eshelby line is regarded as constant corresponding to neglecting the time dependent stiffness of the surrounding material. As the inclusion strain approaches $\gamma_{B'}$, the instability point predicted by the drained analysis, rapid deformation induces undrained response of the inclusion material. Consequently, the inclusion material does not follow the stress strain curve for drained response (dashed curve) but rather that for undrained response; instability is delayed from B' to D' where the tangent to the dilatantly hardened response curve has fallen to the slope of the Eshelby line.

Although both Figure 3 and Figure 4 indicate an increase in τ_∞ during the delay from point B' to point D' (The stiffness changes and increases of τ_∞ are greatly exaggerated for illustration), the deformation is self-driving once the inclusion strain has exceeded $\gamma_{B'}$; that is, after this point, the inclusion strain will accelerate to instability at D' even if τ_∞ is held constant (1, 21). The time which elapses during this period is defined as the precursor time. There is, of course, some arbitrariness in this definition but it is unambiguous in the context of this model and the definition is motivated by the fact that during this period the deformation will be much more rapid than the tectonic strain rate. Consequently, the detection of precursory phenomena may be possible during this period.

To predict the precursor time and to analyze quantitatively the increase of inclusion strain toward instability, it is necessary to obtain Eshelby relations analogous to (5) for a linear porous elastic fluid-infiltrated ("Biot") solid. The governing equations for such a solid were first established by Biot (11) and these are reviewed in the next section. The Eshelby relations can, in principle, be obtained by the same steps outlined in the derivation of (5): First, the problem of an ellipsoidal cavity loaded at its boundary is solved; if the resulting (now time-dependent) deformation of the cavity wall is compatible with homogeneous strain of the interior, then the solution for the inclusion can be obtained by superposition. Thus far, however, only the solution for a spherical cavity has been obtained (8). This solution, its use in obtaining

Eshelby relations, and the application of these relations to the analysis of transient stabilization of runaway instability (9) will be reviewed in the following subsections.

Governing Equations for a Biot Solid

Although the governing equations for a linear porous elastic fluid-infiltrated solid were first derived by Biot (11), Rice and Cleary (12) have given a more elucidating rearrangement of these equations. Rice and Cleary (12) demonstrated that in the limits of drained and undrained response, the total stress σ_{ij} is related to the strain of the solid matrix ε_{ij} by the usual relation of linear elasticity; that is

$$\sigma_{ij} = 2G\,[\varepsilon_{ij} + \nu_e\,\varepsilon_{kk}\,\delta_{ij}/(1 - 2\nu_e)] \qquad (20)$$

where δ_{ij} is the Kronecker delta, G is the shear modulus, and ν_e is an effective value of Poisson's ratio. This Poisson's ratio has the value ν for drained response and ν_u for undrained response where $\nu \leq \nu_u \leq 1/2$. The upper limit is attained for separately incompressible constituents and the lower for highly compressible pore fluid. Thus, the source of the elastically stiffer response for undrained conditions, and hence the stabilizing effect, is an increase in the effective value of Poisson's ratio.

More generally, the stress σ_{ij} and the change in fluid mass content per unit volume m are related linearly to the strain ε_{ij} and the alteration in pore fluid pressure p. The pore fluid pressure is defined precisely as the value of the pressure in a reservoir of homogeneous pore fluid which, when connected to a small element of porous material, would equilibrate any fluid mass flux from the element. Such an element, although it may contain several interconnected pores or fissures, would be regarded in this continuum formulation as a "point". Very rapid load alterations, for example, on the time scale of wave propagation, would cause the pressures in these pores or fissures, to be different and, under these circumstances, the characterization of the pore fluid by a single pressure would be inadequate. Cleary (29) and O'Connell and Budiansky (30) have discussed the response in this dynamic regime. Hence, the undrained response which is regarded as instantaneous in the Biot formulation assumes there is sufficient time for pressure equilibration among cavities occupying a single "point".

The complete set of constitutive equations is the following:

$$\sigma_{ij} = 2G\,[\varepsilon_{ij} + \nu\varepsilon_{kk}\,\delta_{ij}/(1 - 2\nu)] - \zeta\,p\,\delta_{ij} \qquad (21)$$

$$m - m_o = \zeta\,\rho\,[\varepsilon_{kk} + \zeta\,p(1 - 2\nu)(1 - 2\nu_u)/2G(\nu_u - \nu)] \qquad (22)$$

$$q_i = -\,\rho\,\kappa\,\partial p/\partial x_i \qquad (23)$$

where m_o is the value of m in the unloaded state, ρ is the mass density of the pore fluid, and (23) is Darcy's law which relates q_i, the mass flow rate in the x_i direction per unit area, to the gradient of pore fluid pressure; κ is a permeability which is often expressed as $\kappa = k/\mu$ where μ is the fluid viscosity and k has the dimensions of length squared (usually measured in millidarcies; 1 md = 10^{-11} cm^2) or as $\kappa = \bar{k}/\rho_o g$ where g is the acceleration due to gravity and $\bar{k}$ has dimensions of velocity; $\zeta = 1 - K/K_s'$ where $K(= 2G(1 + \nu)/3(1 - 2\nu))$ is the bulk modulus of the porous matrix material and K_s' is an empirical constant which, under conditions stated by Rice and Cleary (12) (also see (31)), is identical to the bulk modulus of the solid constituents.

For drained conditions, any alterations in pore fluid pressure are dissipated, $p = 0$, and (21) reduces to (20) with $\nu_e = \nu$. For undrained conditions, there is insufficient time for fluid mass diffusion from material elements, $m = m_o$, and the change in pore fluid pressure is obtained by equating the right hand side of (22) to zero. Substituting the resulting value for p into (21) again reduces this equation to (20) with $\nu_e = \nu_u$.

These constitutive equations must be combined with the strain displacement relation

$$\varepsilon_{ij} = (\partial u_i/\partial x_j + \partial u_j/\partial x_i)/2, \qquad (24)$$

and field equations expressing equilibrium

$$\partial\sigma_{ij}/\partial x_i = 0 \qquad (25)$$

and conservation of fluid mass

$$\underset{\sim}{\nabla} \cdot \underset{\sim}{q} + \partial m/\partial t = 0 \qquad (26)$$

Substituting Darcy's law (23) in this last equation (26) and rearranging by using (25), (21), and (22) yields a homogeneous diffusion equation for the fluid mass content m (12)

$$\nabla^2 m = \frac{1}{c}\,\frac{\partial m}{\partial t} \qquad (27)$$

where $\nabla^2(\ldots) = \partial^2(\ldots)/\partial x_k\,\partial x_k$. The diffusivity c can be expressed as (12)

$$c = \left[2G\,\frac{(1-\nu)}{(1-2\nu)}\right]\left[\frac{\kappa(\nu_u - \nu)}{\zeta^2(1-2\nu)(1-\nu_u)}\right] \qquad (28)$$

where the first term in square brackets is the modulus governing one dimensional straining and is usually called the consolidation coefficient in soil mechanics.

Note that the diffusivity c rather than the permeability κ is the material parameter which sets the time scale of diffusion. Although these quantities are proportional, the diffusivities corresponding to the same value of permeability may be quite different. For example, Rice and Simons (14) give a diffusivity of 10^{-2} cm^2/sec as representative of the elastic behavior of clay corresponding to a permeability $\bar{k} = 10^{-7}$ cm/s (or $k = 0.1$ md); however, for a Ruhr sandstone with a permeability twice that of the clay, Rice and Cleary (12) give a diffusivity of 53 cm^2/s which is more than three orders of magnitude larger than that of the clay.

Values of c determined from laboratory measurements (see (12) for a summary) are typically at least one to two orders of magnitude smaller than values estimated from field observations. Obviously, large joints and fissures which can contribute substantially to fluid transport in the field are not present in laboratory size samples. Based on a variety of fluid observations, Anderson and Whitcomb (32) suggested a field diffusivity of 1 m^2/s and Rice (1) has estimated $c = 0.1$ m^2/s from measurements by Kovach et al. (33) of water level changes in wells. A recent literature survey by Li (see (34)) has indicated that these values are consistent with published evidence on field diffusivities near fault zones.

Rice and Cleary (12) have tabulated values of ν and ν_u (as well as other parameters) inferred from laboratory tests on rock. However, the presence of large joints and fissures also affects the values of ν tending to reduce ν and increase ν_u (9, 12, 30, 35).

Unfortunately, there appears to be no direct source of field values for these parameters. Neither corresponds to values inferred from seismic wave speed ratios. Rice and Rudnicki (9) have given some estimates by using the self-consistent calculations of O'Connell and Budiansky (35) and a value of crack density parameter suggested by them on the basis of a comparison of their calculations with observations of wave speed ratios prior to the San Fernando earthquake.

Eshelby Relations for a Fluid-Infiltrated Solid

The Eshelby relations for a spherical inclusion in a fluid-infiltrated solid can be constructed by first solving the equations of the last section for sudden application of traction and pore fluid pressure at the wall of a spherical cavity. The solution for sudden application of pore pressure p_o and purely radial total stress σ_o has been given by Rice and Cleary (12). As discussed in (8), the displacement of the cavity wall is independent of p_o and is compatible with a uniform volume strain of the cavity interior. This strain is related to the applied stress by

$$\varepsilon = (3/4G)\,\sigma_o \tag{29}$$

Comparison with (16) reveals that this agrees exactly with the result for a linear elastic solid. The fluid mass flow out of the cavity can be calculated from the pressure distribution outside the cavity and Darcy's law:

$$q(r = a,t) = -\rho\kappa\,\partial p/\partial r = \rho\kappa[1 + a/(\pi ct)^{1/2}]p_o \tag{30}$$

where q is the radial mass flux and a is the radius of the cavity. Rice et al. (8) show that fluid mass conservation on the surface of the cavity leads to the following expression:

$$\dot{m}(t) = -(3\rho\kappa/a^2)\,p_o\,[1 + a/(\pi ct)^{1/2}] \tag{31}$$

where $\dot{m}(t)$ is now interpreted as the rate at which fluid mass of the cavity increases.

The boundary conditions for sudden application of shear traction to the cavity wall are given by Rice et al. (8) as

$$\left.\begin{aligned} x_i\,\sigma_{ij} &= -x_i\,S_{ij} \\ p &= 0 \end{aligned}\right\} \quad r = (x_i\,x_i)^{1/2} = a,\ t > 0. \tag{32}$$

where S_{ij} is an arbitrary deviatoric tensor, i.e., $\mathrm{tr}\,\underline{S} = S_{kk} = 0$, and x_i/a is the component of the outward unit normal to the cavity surface. Rice et al. (8) constructed the solution by recognizing that material isotropy, spherical symmetry and linearity require the displacement to have the form

$$\underline{u} = \underline{x}\,(\underline{x}\cdot\underline{S}\cdot\underline{x})\,F_1(r,t) + \underline{x}\cdot\underline{S}\,F_2(r,t) \tag{33}$$

where $\underline{x}\cdot\underline{S}\cdot\underline{x} = x_i\,S_{ij}\,x_j$, $r = (x_i\,x_i)^{1/2}$ and $F_1(r,t)$ $F_2(r,t)$ are functions to be determined. For the same reasons, the alteration in fluid mass content must have the form

$$m - m_o = (\underline{x}\cdot\underline{S}\cdot\underline{x})\,g(r,t) \tag{34}$$

where $g(r,t)$ is to be determined. (Note that this function differs slightly from that used in (8)). The unknown functions F_1, F_2, and g can be determined by solving the equations which result from substituting (33) and (34) into the governing equations.

Rice et al. (8) demonstrate that the cavity boundary deforms as if the interior had undergone a uniform deviatoric strain given by

$$2G\,e_{ij} = [\xi_u + f(ct/a^2)(\xi - \xi_u)]\,S_{ij} \text{ at } r = a \tag{35}$$

where $\xi = 2(4 - 5\nu)/(7 - 5\nu)$, $\xi_u = 2(4 - 5\nu_u)/(7 - 5\nu_u)$ and the function $f(ct/a^2)$ has the limiting values $f(0) = 0$ and $f(\infty) = 1$. Hence, the longtime and instantaneous responses are given by the classical elasticity solution with Poisson's ratio equal to its drained and undrained value, respectively. The form of (35) is independent of the boundary condition on the fluid mass at the cavity wall although the specific time-dependence of $f(ct/a^2)$ does depend on this boundary condition. The equation governing the time dependence of the cavity strain is obtained by substituting (34) into the diffusion equation (27)

$$\frac{\partial^2 g}{\partial r^2} - \frac{4}{r}\frac{\partial g}{\partial r} = \frac{1}{c}\frac{\partial g}{\partial t} \tag{36}$$

and this must be solved subject to the initial condition $g(r,t=0) = 0$ (because undrained conditions apply at $t = 0$) and to the boundary condition derived from the second of equations (32). The function $f(ct/a^2)$ is related to $g(a,t)$ through the boundary condition on the traction. For $p = 0$ at the cavity boundary, the function $f(ct/a^2)$ is shown in Figure 5 (As shown in (8), $f(ct/a^2)$ exhibits only a slight dependence on material properties over the range of interest). Note that $f(ct/a^2)$ reaches more than 50% of its drained value for $t = 0.1\,a^2/c$ so that this time rather than a^2/c might be regarded as characteristic.

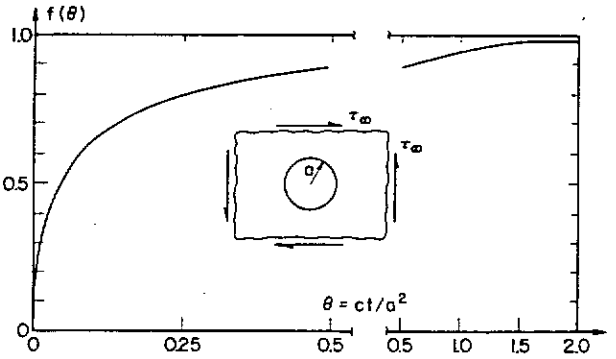

Figure 5. Time dependent shear strain of the cavity wall (r=a) due to sudden application of τ_∞. $f(ct/a^2) = [\gamma(a,t) - \gamma(a,0)]/[\gamma(a,\infty) - \gamma(a,0)]$ From (8).

The solutions (29), (31), and (35) can be generalized by straightforward superposition to arbitrary time variation of the loads at the cavity boundary. The Eshelby relations for the spherical inclusion are then obtained by combining these solutions with those due to uniform stress and strain in the same manner as was done in deriving (5). The resulting Eshelby relations are

$$G[\varepsilon_{inc}(t) - \varepsilon_\infty(t)] = (3/4)\,[\sigma_{inc}(t) - \sigma_\infty(t)] \tag{37}$$

$$\dot{m}_{inc}(t) = -(3\rho\kappa/a^2)\{p_{inc}(t) - p_\infty(t) + \int_{-\infty}^{t} \frac{a}{[\pi c(t-t')]^{1/2}} [\dot{p}_{inc}(t') - \dot{p}_\infty(t')]dt'\} \quad (38)$$

$$G[\gamma_{inc}(t) - \gamma_\infty(t)] = \int_{-\infty}^{t} \{\xi_u + (\xi - \xi_u) f[c(t-t')/a^2]\} \cdot [\dot{\tau}_\infty(t') - \dot{\tau}_{inc}(t')]\, dt' \quad (39)$$

where the last equation, which was derived from (35), has been specialized to a single component of shear. In equation (38) for $\dot{m}_{inc}(t)$, it has been assumed that p_∞ and σ_∞ are such that m_∞ is constant. It has also been assumed that the pore fluid pressure in the inclusion is homogeneous. This cannot, of course, be true exactly but it is likely to be a good approximation if the inclusion is more heavily fissured than the surrounding material as is plausible for the present application.

Equations (37), (38) and (39) relate the state in the inclusion to the state in the far field in a manner which is analogous to (5). If constitutive relations for τ_{inc}, σ_{inc} and m_{inc} are given in terms of γ_{inc}, ε_{inc}, and p_{inc}, these equations (with the linear elastic relations for the surrounding material) are sufficient to determine the time-dependent response of the inclusion in terms of the loads applied in the far field. RR (9) have carried out this procedure to analyze in detail the transient stabilization of runaway instability by coupled deformation diffusion effects. In their analysis, RR (9) consider separately stabilization by the time-dependent stiffness of the surrounding material and by dilatant hardening of the inclusion. Their results are reviewed in the succeeding subsections.

Stabilization by Time-Dependent Stiffness of Surroundings

As shown schematically in Figure 3 and analytically by (35), the unloading stiffness of the material surrounding the inclusion is G/ξ for drained conditions and G/ξ_u for undrained conditions where ξ and ξ_u are given following (35) for the spherical inclusion. Hence, the ratio of drained to undrained response is ξ/ξ_u and since $\xi_u < \xi$, instability can be delayed as shown in Figure 3. Based on the earlier mentioned estimates of in situ values for ν and ν_u, RR suggest that representative values of ξ/ξ_u lie in the range from 1.10 to 1.25.

If dilatant hardening of the inclusion is neglected, the stabilization by time-dependent stiffness can be addressed with reference to equation (39) without regard to (37) and (38). Specifying a constitutive relation for τ_{inc} versus γ_{inc} in (39) yields a nonlinear integral equation for the time-dependent strain in the inclusion. RR use (9) for τ_{inc} versus γ_{inc} and express the result for γ_{inc} in nondimensional form as

$$\frac{\gamma_{inc} - \gamma_p}{\gamma_{D'} - \gamma_p} = \Gamma(\theta;\ R,\ \xi/\xi_u,\ \xi) \quad (40)$$

where $\gamma_{D'}$ is the strain at which instability occurs, $\theta = ct/a^2$ is time nondimensionalized by the diffusion time and

$$R = \xi(1 + \xi)(a^2/c)(\dot{\tau}_\infty/G\lambda)$$

is a nondimensional forcing term which is proportional to the product of the diffusion time a^2/c and the far field stress rate $\dot{\tau}_\infty$. Because the tectonic stress rate represented by $\dot{\tau}_\infty$ is very small (measurements of strain accumulation in Southern California suggest $\dot{\tau}_\infty \simeq 10$ kPa/year (0.1 bar/year) (24, 25)), R is typically a small number and RR investigated values ranging from 10^{-4} to 3. The solution was found to be relatively insensitive to the value of ξ. A representative result is shown schematically in Figure 6 where the dashed curve shows the response in the absence of pore fluid effects. The nondimensional precursor time $\theta_{prec} = ct_{prec}/a^2$ is defined as the time which elapses between the point B' at which runaway would have occurred in the absence of pore fluid effects and final instability, at D'. RR give a plot of θ_{prec} versus R for $\xi/\xi_u = 1.10$ and $\xi/\xi_u = 1.25$. Although the dimensional precursor time t_{prec} does increase with the size of the inclusion zone, it is not proportional to the diffusion time a^2/c: the precursor time increases much more slowly with inclusion size than does the diffusion time. RR give extensive numerical results for representative ranges of parameters. The parameters describing the inclusion stress strain curve are taken to be the following: $\tau_p = 100$ MPa (= 1kbar), $\lambda = 2.5 \times 10^{-3}$, $\gamma_p = 6.25 \times 10^{-3}$ and $G = 20$ GPa (= 200 kbar). For inclusion radii of 1 to 5 km, $\dot{\tau}_\infty = 0.1$ MPa/year (1 bar/year), $c = 0.1$ m^2/sec and 1.0 m^2/sec, and $\xi/\xi_u = 1.10$ and 1.25, they find precursor times of 15-400 days based on stabilization by time-dependent stiffness of the surroundings, although they suggest that the lower limit may be more indicative of when precursory variations could easily be detected.

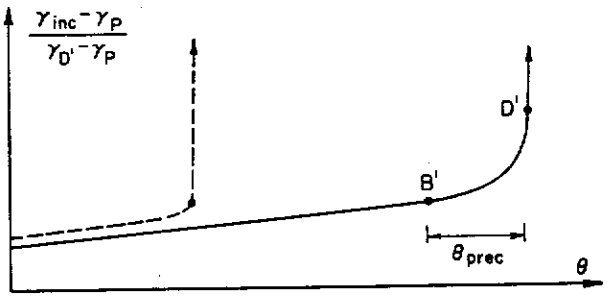

Figure 6. Typical postpeak variation of inclusion strain with $\theta = ct/a^2$ as calculated in (9) for stabilization by the time dependent stiffness effect. Far field loading rate is constant. Dashed curve shows drained response (as in Figure 2). Points B' and D' correspond to points in Figure 3. For numerical values, see (9).

Rice (1) has also calculated precursor times for the time-dependent stiffness mechanism by approximating the response function $f(\theta)$ in (39) by

$$f(\theta) = 1 - e^{-\alpha\theta}$$

where α is chosen to give the best fit. This corresponds to approximating the actual response of a fluid-infiltrated solid by that of a standard linear solid with long and short time responses chosen to coincide with drained and undrained behavior, respectively. Although the approximation to $f(\theta)$ is not a particularly good one, the precursor times calculated by Rice (1) agree well with those calculated by RR. Because this

approximation does result in a great saving of computation time, it may be useful in future calculations.

Stabilization by Dilatant Hardening

For the analysis of dilatant hardening, it is necessary to generalize the constitutive relations (equations (14) and (15)) of the inclusion to include the effects of variations in pore fluid pressure. This can be accomplished by using the effective stress principle: the hydrostatic stress σ is to be replaced in (14) and (15) by a linear combination of σ and p. For elastic deformation Nur and Byerlee (31) (also see (12)) have shown that the correct form of the effective stress is

$$\sigma - (1 - K/K_s)p$$

where, as before, K is the bulk modulus of the matrix material and K_s is the bulk modulus of the solid constituents. This form of the effective stress assumes isotropic behavior, but Carroll (36) has given the generalization for anisotropy. Rice (37) has shown that for inelastic deformation typical of brittle rock, that is, inelastic deformation arising from frictional sliding at sharp asperity contacts and microcracking from sharp-tipped fissures, the appropriate form of the effective stress is $\sigma - p$. Making these replacements in (14) and (15) yields

$$\dot{\gamma} = \dot{\tau}/G + [\dot{\tau} - \mu(\dot{\sigma} - \dot{p})]/h \tag{41}$$

$$\dot{\epsilon} = -[\dot{\sigma} - (1 - K/K_s)\dot{p}]/K + \beta[\dot{\tau} - \mu(\dot{\sigma} - \dot{p})]/h \tag{42}$$

where the subscript "inc" has been omitted. One additional constitutive equation is needed for m the change in fluid mass content per unit volume. The fluid mass content is related to the apparent volume fraction v by $m = \rho v$. Linearizing this relation yields

$$dm = v_o\, d\rho + \rho_o\, dv \tag{43}$$

where the subscript "o" denoting the reference value will be implicit in the subsequent equations. The change in density is given

$$d\rho = \rho \frac{dp}{K_f} \tag{44}$$

where K_f is the bulk modulus of the pore fluid. The increment of apparent volume fraction can be written as the sum of elastic and inelastic portions: The elastic portion can be expressed in terms of stresses by using reciprocity relations (38, 20) and Rice (20, 37) has shown that $dP_v = dP_\epsilon$ under the same circumstances for which $\sigma - p$ is the appropriate form of the effective stress. The final result is

$$\frac{\dot{m}}{\rho} = \frac{v\dot{p}}{K_f} - \left[\frac{1}{K} - \frac{1}{K_s}\right](\dot{\sigma} - \dot{p}) - \frac{v}{K_s}\dot{p} + \beta[\dot{\tau} - \mu(\dot{\sigma} - \dot{p})]/h \tag{45}$$

The stabilizing effect of dilatant hardening can be illustrated simply from (41), (42) and (45) before considering the more complicated results of the inclusion model. For drained conditions, $p = 0$ and $d\tau/d\gamma$ is given by (12) (with $\dot{\sigma} = 0$, for convenience). If, however, the response is undrained, $\dot{m} = 0$ and the resulting value of p can be calculated from (45):

$$\dot{p} = -\beta K' \dot{\tau}/(h + \mu\beta K') \tag{46}$$

where again for convenience, $\dot{\sigma} = 0$ and the modulus K' is defined by the following expression:

$$\frac{1}{K'} = \frac{1}{K} + \frac{v}{K_f} - \frac{1 + v}{K_s} \tag{47}$$

Substituting (46) into (41) with $\dot{\sigma} = 0$ reveals that $d\tau/d\gamma$ is given by an expression analogous to (12) but with the hardening modulus h replaced by the augmented value $h + \mu\beta K'$, that is,

$$(d\tau/d\gamma)_{undrained} = \frac{h + \mu\beta K'}{1 + (h + \mu\beta K')/G} \tag{48}$$

For representative values of μ, β and K' this increase in h can be significant. For heavily fissured rock in which most of the porosity is due to long narrow cracks and a pore fluid bulk modulus comparable to that of liquid water ($K_f = 2.2$ GPa (= 22 kbar)), $K' \approx K$. If, however, K_f is reduced by high temperatures, low pore pressure or entrapped gases $K' \approx K_f/v$. Of course, for the inclusion model, the above result is modified by the effects due to the constraint of the surrounding material. In particular, RR show that for the inclusion model the undrained response is given by (48) with K' replaced by

$$K_f' = M\{1 + (K/M)\,[(vK/K_f)(M_s/M)(1-K_f/K_s) + (1-K/K_s)]^{-1}\} \tag{49}$$

where $M = K/(1 + 3K/4G)$, $M_s = K_s/(1 + 3K_s/4G)$ and K_f' exhibits the same limiting behavior as K'.

RR give a full analysis of dilatant hardening for the inclusion and the details will not be discussed here. Because they neglect the time-dependent stiffness effects which were discussed earlier, they use (6) rather than (39) as the Eshelby relation for shear. Equation (6) is used with the other Eshelby relations (37) and (38) and with the constitutive relations (41), (42), and (45) to obtain a set of two coupled equations, an ordinary differential equation and an integral-differential equation, which describe the time dependent response of the inclusion material. The τ_{inc} versus γ_{inc} curve is again chosen to be that given by (9) and because this is assumed to be the relation appropriate for in situ response, the slope of this curve is related to h as indicated following (18), that is

$$\frac{d\tau_{inc}}{d\gamma_{inc}} = \frac{h + \mu\beta M}{1 + (h + \mu\beta M)/G} \tag{50}$$

A schematic representation of the results for the time variation of postpeak inclusion strain is shown in Figure 7. Also shown in Figure 7 is the decrease of inclusion pore fluid pressure from its value at peak stress. As shown, the decrease is extremely slow until very near instability. In both cases plotted by RR, p has decreased by less than 1 MPa (10 bars) by the time at which instability would have occurred in the absence of pore fluid effects. This result suggests that precursory effects due to the decrease in pore fluid pressure (e.g., a change in wave speed ratios due to vaporization of existing pore fluid (32)) may be observable only very near to instability.

RR also give a plot of θ_{prec} versus the nondimensional strain-rate $\dot{\gamma}_\infty\, t_D$. As in the case of stabilization by the time dependent stiffness effect, the length of the precursor time increases with increasing size of the inclusion although again the precursor time is not proportional to a^2. For the same τ_{inc} versus γ_{inc} curve, the precursor times predicted for stabilization by dilatant hardening are generally greater than

those predicted for the time-dependent stiffness effects. However, RR have suggested that the dilatant hardening calculations may produce upper estimates of the precursor time because the effects of nonlinear fluid compressibility at low pressure were neglected and the values of the dilatancy factor inferred from laboratory results may be much larger than those in situ. Nevertheless, the calculations do indicate that even very small amounts of dilatancy (too small to cause observable changes in seismic wave speed travel times) can have a dramatic effect on the evolution of runaway instability.

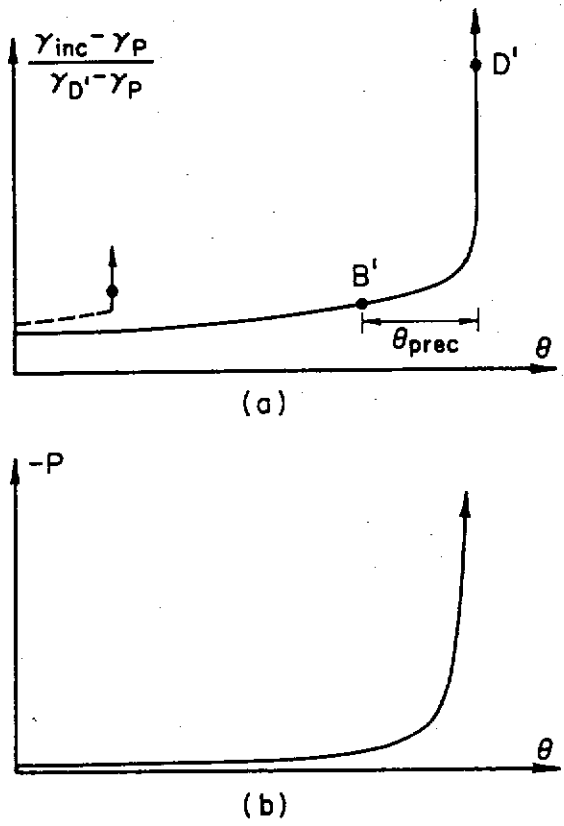

Figure 7. (a) Typical variation of inclusion strain with $\theta = ct/a^2$ as calculated in (9) for stabilization by dilatant hardening effect. Far field loading rate is constant. Dashed curve shows drained response (as in Figure 2). Points B' and D' correspond to points in Figure 4. (b) Decrease in inclusion pore pressure as instability is approached. For numerical values, see (9).

Experiments on Dilatant Hardening. Reynolds (16) has described a number of simple laboratory experiments which illustrate the dilatant hardening of granular materials and Brace and Martin (18) have observed dilatant hardening in axisymmetric compression tests on brittle rock. The experiment of Brace and Martin (18) was actually concerned with investigating the "effective stress principle" which, in this context, states that the deviatoric stress at which failure occurs is unaltered by increases of equal amounts in the confining stress and pore fluid pressure. They observed agreement with this principle at low strain-rates but at higher strain-rates they observed a strengthening which they attributed to dilatant hardening. However, the analysis of RR indicates that the coupling of dilatancy and pore fluid diffusion, in addition to delaying the onset of instability, or strengthening the rock mass, can set the time scale of the failure process. Recently, Martin (19) has examined more closely this aspect of stabilization by pore fluid effects in axisymmetric compression tests on Westerly granite. Martin's (19) results will be reviewed here and discussed in the context of the predictions of RR.

Martin (19) conducted axisymmetric compression tests on fluid saturated samples of Westerly granite at different strain-rates, confining pressures, and pore-fluid pressures. Each sample was deformed at constant confining pressure and constant load rate although near instability (within several minutes of failure) the actual loading rate deviated from the prescribed value because of the inability of the loading apparatus to keep up with the rapid deformation of the sample. During each experiment, the pore fluid pressure in a reservoir attached to one end of the sample was held constant. (Of course, the actual pore fluid pressure in the sample will differ from that in the reservoir if dilatancy occurs at a rate faster than pore fluid can diffuse into the sample). Typical results for the time variation of nominal axial strain are shown in Figure 8 for different values of the effective confining stress $\bar{\sigma}_c$ (confining stress minus pore fluid pressure) and ratios of reservoir pore fluid pressure p_{rev} to confining stress σ_c. Figure 8 has been replotted from Figure 1 of Martin (19) in terms of the nominal axial strain (axial displacement divided by the sample length $\ell = 3.81$ cm) and time nondimensionalized by the diffusion time ℓ^2/c where $c = 0.22$ cm^2/sec, given by Rice and Cleary (12) for Westerly granite. Martin (19) discusses the results in terms of a qualitative classification of the curves as stable, unstable (Martin uses "dynamic"), or transitional. Curve (a) (for $\bar{\sigma}_c = 10^2$ MPa (1 kbar) and $p_{rev}/\sigma_c = 0.20$) represents unstable behavior: there is an abrupt acceleration of strain terminated by an audible fracture (indicated by the dashed line in Figure 8). Curve (c) (for $\bar{\sigma}_c = 50$ MPa (500 bars), $p_{rev}/\sigma_c = 0.64$) represents stable behavior: there is a relatively long period of accelerating strain followed by inaudible fracture. Curve (b) (for $\bar{\sigma}_c = 10^2$ MPa (1 kbar), $p_{rev}/\sigma_c = 0.6$) illustrates transitional behavior.

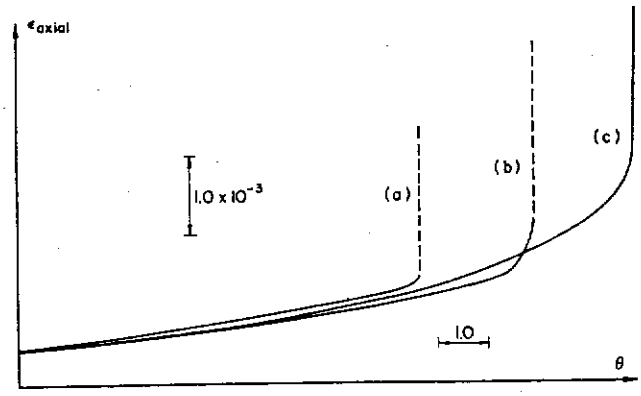

Figure 8. Variation of nominal axial strain ϵ_{axial} with $\theta = ct/\ell^2$ ($c = 0.22$ cm^2/sec, $\ell = 3.81$ cm) observed by Martin (19). Redrawn from Figure 1 of (19) so that curves coincide at left hand edge.

In spite of obvious differences between the experimental configuration and the model analyzed by RR, the time variation of nominal axial strain in Figure 8 is qualitatively very similar to the variation of inclusion shear strain predicted by RR. Martin's qualitative classification of stable or unstable corresponds roughly to the length of the precursor time: short or nonexistent precursor times would be classified as unstable; long precursor times correspond to stable behavior (Obviously, the classification depends to some extent on the time scale of interest).

Martin (19) also plots the stress difference at failure against the ratio p_{rev}/σ_c and finds that the transition from unstable to stable behavior occurs at lower values of the stress difference for higher values of p_{rev}/σ_c. Moreover, the value of p_{rev}/σ_c at which the transition occurs increases with strain-rate. These trends appear to be due to the limit on the pore pressure decrease and, hence, on dilatant hardening, which is imposed by the ambient level of pore fluid pressure in the sample. In the calculations of RR, the bulk modulus of the pore fluid was assumed to be constant and consequently the decrease of pore fluid pressure could become unbounded as instability was approached. If, however, effects of nonlinear fluid compressibility had been included, the bulk modulus of the pore fluid K_f would vanish when the absolute magnitude of the pore pressure neared zero, that is, when the pore fluid pressure decrease equals in magnitude the ambient value of pore pressure (or, perhaps, well before this point if decreases in pressure cause substantial exsolution of gases). Because the dilatant hardening effect vanishes in the limit as K_f goes to zero (see discussion following (48) and (49)), runaway instability would occur at this point and the precursor times would be shorter for decreasing values of the ambient pressure.

Stabilization of Narrow Inclusion Zones

The results of RR apply rigorously only for spherical zones. For very narrow zones, the inclusion model may be inappropriate: the stress concentrations near the ends of the zone may cause the zone to spread. In this case a model of a spreading crack-like zone of inelasticity (1, 2, 14; also, Rice, this volume) may be more suitable. Nevertheless, it is still of interest to consider the inclusion model for narrow zones because, at the very least, the predictions are relevant to assessing conditions for the initiation of narrow spreading zones.

For the stabilization of runaway instability by the time dependent stiffness effect, RR obtained approximate results for narrow inclusion zones simply by using an appropriate value of ξ. As mentioned following (7), $\xi = 10$ for a narrow axisymmetric inclusion of aspect ratio $a/b \simeq 18$. The predicted time variation of inclusion strain for narrow zones is similar to that for spherical zones, but RR find that the precursor times for the narrow zone are 10 to 20 times smaller.

Rudnicki (7) has also given a direct plane strain analysis for the stabilization of slip on a frictional surface by the time dependent stiffness effect. He simulated the fault by two edge dislocations of opposite sign with the distance between them chosen so that the relative slip midway between the dislocations is equal to that at the center of a crack of length 2L. Rudnicki (7) obtained an Eshelby relation analogous to (39) by using the plane strain solution of Rice and Cleary (12) for a dislocation suddenly introduced into a Biot solid (The solution for the special case of incompressible solid and fluid constituents was obtained in (13)). The constitutive response was specified as a relation for the shear stress on the fault as a function of the relative slip δ. Qualitatively, the results are similar to those of the inclusion model. Moreover, if the parameters of τ versus γ relation are chosen to be consistent with the τ versus γ relation for a narrow inclusion (Even though, as noted by Rudnicki (7), there seems to be some discrepancy when constitutive parameters estimated from experiments on intact rock are applied to deformation of narrow zones and compared with parameters estimated from frictional sliding experiments) the predictions for the precursor time are in good quantitative agreement. This agreement is in spite of the fact that the calculation of Rudnicki (7) was for plane strain whereas that of RR simulated a narrow axisymmetric fault zone. Generally, however, the precursor times predicted by Rudnicki (7) are very short, typically less than a few days for a plausible range of parameters describing the τ versus δ relation, fault lengths of 1 to 5 km., a tectonic stress rate of 10 kPa/year (0.1 bar/year) and field diffusivities of 0.1 to 1.0 m^2/sec.

One particularly interesting feature of the calculation of Rudnicki (7) for slip on a frictional surface is that the dimensional precursor time t_{prec} can decrease with increasing fault length L. This result contradicts the expectation that the precursor time should scale roughly as the diffusion time which is proportional to L^2/c. Nevertheless, this result can be rationalized by a simple dimensional analysis. The nondimensional precursor time $\theta_{prec} = ct_{prec}/L^2$ can be expressed as

$$\theta_{prec} = F[Q; (1 - \nu)/(1 - \nu_u)]$$

where Q is a nondimensional driving force which is proportional to the far field stress rate $\dot{\tau}_\infty$ and may, in addition, be a function of the various nondimensional groups which enter the problem. This dependence can be expressed as

$$Q = f[\nu, \nu_u, \dot{\tau}_\infty L^2/cG, L/\delta^*, \Delta\tau/G]$$

where $\Delta\tau$ is the difference between peak and residual values of friction stress, δ^* is the amount of slip on the fault which is necessary to reduce the shear stress there from the peak value to the residual value, and the remaining quantities have been defined previously. The presence of the nondimensional length L/δ^* introduces the possibility that Q will increase faster with L than does the diffusion time. In particular, Rudnicki (7) assumes a quadratic τ versus δ relation and in this case Q has the following form

$$Q \propto (\dot{\tau}_\infty L^2/cG)(\Delta\tau/G)(L/\delta^*)^2$$

Because Q is proportional to L^4 whereas the diffusion time is proportional to L^2, increasing L causes the driving force to increase faster than the diffusion time and, consequently, results in a decrease of the precursor time with L, at least for a range of parameters.

As yet, there has been no complete analysis of coupled deformation diffusion effects associated with dilation of a narrow fault zone. Rudnicki (21) (also see (39)) has given some preliminary analysis which suggests that the dilatant hardening effect is extremely strong for very narrow zones. This strong effect may, however, be mitigated by the fact that shear of a narrow zone or slip on a surface may be able to generate only a limited amount of dilatancy. In addition to the dilatant hardening effect, there is also an effect due to the time dependent response of the material surrounding the fault to uplift on the fault surface (This effect did not appear in the analysis of spherical

inclusions because the response to hydrostatic stress (see eq. (37)) is the same for drained and undrained conditions). This effect turns out to be destabilizing in the sense that the effective compressive stress on the fault is less for undrained response than for drained response. Nevertheless, the preliminary indications are that this effect will be overwhelmed by the stabilizing effect of dilatant hardening.

CONCLUDING DISCUSSION

This paper has reviewed some predictions for processes preparatory to earthquake faulting based on modeling a fault zone as an embedded inclusion. The model is intended to apply to shallow crustal events for which the rock responds in an essentially brittle fashion and for which the boundary condition at the bottom of the lithosphere enters only in determining the far field stress rate. Because the rock mass has been assumed to be unbounded, the analysis applies strictly to earthquake events which are small enough that effects of the free surface are not significant.

For fault zone material which is strain-softening, as is typical of brittle rock, the model predicts that runaway instability will be preceded by an acceleration of inclusion shear strain. If the deformation of the rock mass is coupled to the diffusion of an infiltrating pore fluid, then instability can be delayed for a length of time, which is defined as the precursor time, and the acceleration of strain prior to instability is more pronounced.

The precursory effects described here are short-term, on the time scale of days rather than years. For a spherical inclusion zone of radius 1 km., RR give 2 to 10 days as a minimum estimate of the time period prior to instability during which precursory effects are likely to be detectable. For very narrow zones, this time period will be shorter although in this case, a spreading crack-like zone of inelasticity is probably a more appropriate model than an inclusion zone.

The precursory acceleration of inclusion shear strain may be detectable as an increased rate of deformation (tilt or strain) of the ground surface although the magnitude of the effect will decrease roughly as the inverse square of distance from the fault zone. Changes in physical properties due to the microcracking which accompanies the inelastic straining may provide more easily detectable precursors. The calculations of RR suggest that relatively large amounts of dilatancy are needed to cause changes in seismic properties by the undersaturation of fluid-infiltrated rock. However, transport properties may be affected by smaller amounts of microcracking causing changes in restivity (40) or radon content of wells (41). Moreover, resistivity changes may be augmented by the flow of pore fluid induced by deformation of the inclusion zone.

The model which has been reviewed here is a simple one and more elaborate models could be constructed. Coupled deformation diffusion effects have been analyzed precisely only for spherical inclusions and the effects of geometry could be considered more carefully. A full analysis of the effect of localization of deformation on the subsequent response of the inclusion has not yet been given. It may be that localization of deformation initiates a spreading crack-like zone of inelasticity, prior to the onset of runaway, rather than simply modifying the bulk response of the inclusion material as assumed by RR. In any case, the results of Rice and Simons (14) for stabilization of a spreading fault by the time dependent stiffness effect are promising and this is an area that would seem to merit more attention. However, at present, the most pressing need seems to be for more accurate values of material and transport properties, particularly values appropriate to in situ behavior.

ACKNOWLEDGEMENT

Support during the preparation of this review was provided by the U.S. Geological Survey National Earthquake Hazards Reduction Program and by the Department of Theoretical and Applied Mechanics at the University of Illinois.

REFERENCES

1. Rice, J. R., "Theory of Precursory Processes in the Inception of Earthquake Rupture," Gerlands Beitr. Geophysics, Vol. 88, 1979, pp. 91-127.

2. Rice, J. R., "The Mechanics of Earthquake Rupture," Proceedings of the International School of Physics "Enrico Fermi", Italian Physical Society, Course LXXVIII (1979, Varenna on Lake Como, Italy) on Physics of the Earth's Interior, edited by E. Boschi, North-Holland Publishing Co., publication expected, 1980-81.

3. Rudnicki, J. W., "The Inception of Faulting in a Rock Mass With a Weakened Zone," Journal of Geophysical Research, Vol. 82, 1977, pp. 844-854.

4. Stuart, W. D., "Strain Softening Instability Model for the San Fernando Earthquake," Science, Vol. 203, 1979, pp. 907-910.

5. Stuart, W. D., "Strain Softening Prior to Two-Dimensional Strike-Slip Earthquakes," Journal of Geophysical Research, Vol. 84, 1979, pp. 1063-1070.

6. Stuart, W. D. and Mavko, G. M., "Earthquake Instability on a Strike-Slip Fault," Journal of Geophysical Research, Vol. 84, 1979, pp. 2153-2160.

7. Rudnicki, J. W., "The Stabilization of Slip on a Narrow Weakening Fault Zone by Coupled Deformation-Pore Fluid Diffusion," Bulletin of the Seismological Society of America, Vol. 69, 1979, pp. 1011-1026.

8. Rice, J. R., Rudnicki, J. W., and Simons, D. A., "Deformation of Spherical Cavities and Inclusions in Fluid-Infiltrated Elastic Materials," International Journal of Solids and Structures, Vol. 14, 1978, pp. 289-303.

9. Rice, J. R. and Rudnicki, J. W., "Earthquake Precursory Effects Due to Pore Fluid Stabilization of a Weakening Fault Zone," Journal of Geophysical Research, Vol. 84, 1979, pp. 2177-2193.

10. Terzaghi, K. and Peck, R. B., Soil Mechanics in Engineering Practice, 2nd Edition, Wiley, New York 1967.

11. Biot, M. A., "General Theory of Three Dimensional Consolidation," Journal of Applied Physics, Vol. 12, 1941, pp. 155-164.

12. Rice, J. R. and Cleary, M. P., "Some Basic Stress Diffusion Solutions for Fluid-saturated Elastic Porous Media With Compressible Constituents," Reviews of Geophysics and Space Physics, Vol. 14, 1976, pp. 227-241.

13. Booker, J. R., "Time-dependent Strain Following Faulting of a Porous Medium," Journal of Geophysical Research, Vol. 79, 1974, pp. 2037-2044.

14. Rice, J. R. and Simons, D. A., "The Stabilization of Spreading Shear Faults by Coupled Deformation-Diffusion Effects in Fluid-Infiltrated Porous Materials," Journal of Geophysical Research, Vol. 81, 1976, pp. 5322-5334.

15. Ruina, A., "Influence of Coupled Deformation-Diffusion Effects on Retardation of Hydraulic Fracture," in Proceedings of the 19th U.S. Symposium on Rock Mechanics, Stateline, Nevada, edited by Y. S. Kim, 1978, pp. 274-282.

16. Reynolds, O., "On the Dilatancy of Media Composed of Rigid Particles in Contact, With Experimental Illustrations," Philosophical Magazine, 1885. (Reprinted in Papers on Mechanical and Physical Subjects by O. Reynolds, Vol. 2, Cambridge University Press, New York, 1901, pp. 203-216.

17. Frank, F. C., "On Dilatancy in Relation to Seismic Sources," Reviews of Geophysics and Space Physics, Vol. 3., 1964, pp. 485-503.

18. Brace, W. F. and Martin, R. J., "A Test of the Law of Effective Stress for Crystalline Rocks of Low Porosity," International Journal of Rock Mechanics and Mining Sciences, Vol. 5, 1968, pp. 415-426.

19. Martin, R. J., "Pore Pressure Stabilization of Failure in Westerly Granite," Geophysical Research Letters, Vol. 7, 1980, in press.

20. Rice, J. R., "On the Stability of Dilatant Hardening for Saturated Rock Masses," Journal of Geophysical Research, Vol. 80, 1975, pp. 1531-1536.

21. Rudnicki, J. W., "Localization of Deformation, Brittle Rock Failure, and Model for the Inception of Earth Faulting," Ph.D. Thesis, Brown University, Providence, RI, 1977.

22. Eshelby, J. D., "The Determination of the Elastic Field of an Ellipsoidal Inclusion and Related Problems," Proceedings of the Royal Society of London, Series A, Vol. 241, 1957, pp. 376-396.

23. Eshelby, J. D., "Elastic Inclusions and Inhomogeneities," in Progress in Solid Mechanics, edited by I. N. Sneddon and R. Hill, Vol. 2, North Holland, Amsterdam, 1961, pp. 88-140.

24. Prescott, W. H. and Savage, J. C., "Strain Accumulation on the San Andreas Fault Near Palmdale, California," Journal of Geophysical Research, Vol. 81, 1976, pp. 4901-4908.

25. Savage, J. C. and Prescott, W. H., "Geodimeter Measurements of Strain During the Southern California Uplift," Journal of Geophysical Research, Vol. 84, 1979, pp. 171-177.

26. Rudnicki, J. W. and Rice, J. R., "Conditions for the Localization of Deformation in Pressure-sensitive Dilatant Materials," Journal of the Mechanics and Physics of Solids, Vol. 23, 1975, pp. 371-394.

27. Cleary, M. P. and Rudnicki, J. W., "The Initiation and Propagation of Dilatant Rupture Zones in Geological Materials," in The Effects of Voids on Material Deformation, edited by S. C. Cowin, Am. Soc. Mech. Engr. Appl. Mech. Division, Vol. 16, New York, 1976, pp. 13-30.

28. Walsh, J. B., "Stiffness in Faulting and in Friction Experiments," Journal of Geophysical Research, Vol. 76, 1971, pp. 8597-8598.

29. Cleary, M. P., "Heterogeneity and Porosity Effects on the Response of Geomaterials," in Advances in Civil Engineering Through Engineering Mechanics, American Society of Civil Engineers, New York, 1977, pp. 360-363.

30. O'Connell, R. J. and Budiansky, B., "Visco-Elastic Properties of Fluid-saturated cracked solids," Journal of Geophysical Research, Vol. 82, 1977, pp. 5719-5735.

31. Nur, A. and Byerlee, J. D., "An Exact Effective Stress Law for Elastic Deformation of Rock With Fluid," Journal of Geophysical Research, Vol. 76, 1971, pp. 6414-6419.

32. Anderson, D. L. and Whitcomb, J. H., "Time-dependent Seismology," Journal of Geophysical Research, Vol. 80, 1975, pp. 718-732.

33. Kovach, R. L., Nur, A., Wesson, R. L. and Robinson, R., "Water-level Fluctuations and Earthquakes on the San Andreas Fault Zone," Geology, Vol. 3, 1975, pp. 437-440.

34. Rice, J. R. and Simons, D. A., "Fundamentals of Deformation and Rupture Processes in Porous Geological Materials, Summary of Work on U.S.G.S. contract 14-68-0001-15866 Mod.1 at Brown University," in Summary of Technical Reports of Participants in National Earthquake Hazards Reduction Program, Vol. 4, U.S. Geological Survey, Office of Earthquake Studies, Menlo Park, CA., December, 1978, p. 500.

35. O'Connell, R. J. and Budiansky, B., "Seismic Velocities in Dry and Saturated Cracked Solids," Journal of Geophysical Research, Vol. 79, 1974, pp. 5412-5426.

36. Carroll, M. M., "An Effective Stress Law for Anisotropic Elastic Deformation," Journal of Geophysical Research, Vol. 84, 1979, pp. 7510-7512.

37. Rice, J. R., "Pore Pressure Effects in Inelastic Constitutive Formulations for Fissured Rock Masses," in Advances in Civil Engineering Through Engineering Mechanics, American Society of Civil Engineers, New York, 1977, pp. 360-363.

38. Biot, M. A., "Nonlinear and Semilinear Rheology of Porous Solids," Journal of Geophysical Research, Vol. 78, 1973, pp. 4924-4937.

39. Minster, J. B. and Rudnicki, J. W., "Theoretical Studies in the Role of Pore Fluid in Premonitory Phenomena," Final Technical Report on U.S. Geological Survey, Contract No. 14-08-0001-16795 to California Institute of Technology, June, 1979.

40. Mazella, A. and Morrison, H. F., "Electrical Resistivity Variations Associated With Earthquakes on the San Andrea Fault," Science, Vol. 185, 1974, pp. 855-857.

41. Wakita, H., Nakamura, Y., Notsu, K., Noguchi, M., Asada, T., "Radon Anomaly: A Possible Precursor of the 1978 Izu-Oshima-kinkai Earthquake," Science, Vol. 207, 1980, pp. 882-883.